Journal of Power Sources 199 (2012) 373–378

Contents lists available at SciVerse ScienceDirect

Journal of Power Sources

journal homepage: www.elsevier.com/locate/jpowsour

Enhancement of capacitance performance of flexible carbon nanofiber paper by adding graphene nanosheets

Zhixin Tai [a,b], Xingbin Yan [a,*], Junwei Lang [a], Qunji Xue [a]

[a] State Key Laboratory of Solid Lubrication, Lanzhou Institute of Chemical Physics, Chinese Academy of Sciences, Lanzhou 730000, China
[b] Graduate University of Chinese Academy of Sciences, Beijing 100080, China

ARTICLE INFO

Article history:
Received 6 July 2011
Received in revised form
29 September 2011
Accepted 4 October 2011
Available online 10 October 2011

Keywords:
Carbon fiber
Graphene
Composite
Supercapacitor

ABSTRACT

In this work, a flexible and freestanding carbon nanofiber/graphene nanosheet (CNF/GNS) composite paper is prepared via electrospinning followed by high-temperature annealing using a polyacrylonitrile/GNS/dimethylformamide mixture as electrospun precursor. The structure characterizations show that GNS homogeneously distributes in the CNF, forming a thin, light-weight and flexible composite paper. Due to the reinforcing effects coming from CNF and GNS, the Brunauer Emmett Teller (BET) specific surface area, conductivity and capacitance performance of pure CNF are significantly improved after adding GNS. The GNS/CNF composite paper exhibits the largest specific capacitance of 197 F g^{-1}, about 24% higher than that of pure CNF paper. Therefore, based on the above investigations, such GNS/CNF composite paper can be a potential candidate for high-performance flexible capacitors.

1. Introduction

Flexible electrochemical supercapacitors, shown to be promising modern energy storage systems, have aroused wide interests for their potential applications in portable electronic devices, hybrid electric vehicles, and medical devices [1,2]. An ideal flexible supercapacitor should hold a combination of excellent mechanical strength and large electrochemical capacitance [3]. Although carbon materials, transition metal oxides and conducting polymers have been widely studied as the electrode material for supercapacitors, only several carbon materials, including carbon nanotubes (CNTs) [4–7], carbon fibers [8–10] and graphene [11], have displayed favorable flexibility and show promising application for freestanding and flexible supercapacitors.

Since graphene nanosheet (GNS) was first isolated in 2004 with the help of scotch tape, researchers have excitedly turned to the material to discover its potential applications. A single layer of carbon atoms whose applications range from ultrafast electronics to biosensors to flexible displays, graphene is strong, light, transparent, and a conductor of heat and electricity [12]. Owing to its excellent electronic transport properties, extremely high mechanical stiffness, exceptional electrical conductivity, high aspect ratio, and relatively low-cost fabrication compared with CNT, GNS has been predicted to hold great promise for supercapacitors. The supercapacitive performance of GNS was first explored by Ruoff and co-workers [13], and they found out that chemically modified graphene (CMG) exhibits large capacitances of 135 F g^{-1} and 99 F g^{-1} in aqueous and organic electrolytes, respectively. This discovery has led to an explosion of interest in the study of graphene-based composites for supercapacitors, such as GNS/conductive polymers, GNS/metal oxides, and GNS/other carbon materials [14–17]. These studies have revealed that the capacitive performance of pristine conductive polymers, metal oxides and carbon materials can be significantly improved by adding GNS [18,19].

As electrode materials, carbon nanofiber (CNF) has been playing the leading role in supercapacitors, due to their high surface area, controllable electronic conductivity, low cost, and simplicity of preparation. However, the application of CNF in supercapacitor is still limited due to the low energy. To improve power and energy density of CNF-based supercapacitors, researchers have put attention to modifying CNF, such as increasing impactful surface area and introduction of other electroactive materials. Therein, CNF-based nanocomposites are of great interest when each constituent component provides specific functions for high performance applications. The nanocomposites of CNF and pseudo-faradic reactions capacitance material, such as manganese dioxide, cobalt oxide [20], nickel oxide [21], polyaniline [22], polycarbazole [23], and polypyrrole [24] have been successfully synthesized. Moreover, carbon–carbon composites are also researched as ideal electrode materials for electrochemical capacitors. The multiwalled carbon

* Corresponding author. Tel.: +86 931 4968055; fax: +86 931 4968055.
E-mail address: xbyan@licp.cas.cn (X. Yan).

0378-7753/$ – see front matter © 2011 Elsevier B.V. All rights reserved.
doi:10.1016/j.jpowsour.2011.10.009

nanotubes/CNF composite was successfully prepared by Guo et al., and the specific capacitance of the composite is up to 310 F g^{-1} at current density of 100 mA g^{-1} [25]. In addition, the influence of oxidation level on the capacitance performance of electrochemical capacitor which prepared from the CNT/CNF composites is studied by Hsieh and his co-workers, and they found that the increase of O/C ratio would further enhance the capacitance of CNT/CNF composites [26]. Nevertheless, little attention has been focused on the supercapacitors application of GNS/CNF composite.

As a simple, convenient, environmental friendly and efficient technique, electrospinning can be used for preparing flexible CNF paper. The main advantage of electrospinning is the ability to produce fibers ranging from nanometer to submicron in diameter. Moreover, the CNF/GNS composite paper can be directly prepared via electrospinning after addition GNS to the electrospun precursor. More importantly, the preparation of flexible and freestanding CNF/GNS composite paper is first demonstrated in this paper. In addition, the electrode preparation process is simple and fast because no binder employed during this process, which not only lowers the preparation costs but also offers advantages in terms of stability and performance.

In this paper, flexible CNF/GNS paper with a small quantity of GNS was prepared using electrospinning method. The obtained composite paper maintains equal pristine flexibility of the CNF paper and displays improved specific surface area and electrochemical performances compared with the pure CNF paper. The GNS/CNF composite paper exhibits the largest specific capacitance of 197 F g^{-1}, about 24% higher than that of pure CNF paper.

2. Experimental

2.1. Materials

PAN (M_w: 80,000–100,000) was purchased from Chinese Jilin Chemical Co., Ltd. N,N-dimethyl formamide (DMF) was purchased from Tianjin Reagent Company. Other reagents were commercially available and were of analytical reagent grade. Twice-distilled water with a resistance about 18 MΩ cm^{-1} was used throughout.

2.2. Preparation of graphene oxide (GO)

In a typical synthesis, graphite powder (3 g, 325 mesh) was put into an 80 °C solution of concentrated H_2SO_4 (12 ml), $K_2S_2O_8$ (2.5 g), and P_2O_5 (2.5 g). The mixture was kept at 80 °C for 4.5 h using a hotplate. Successively, the mixture was cooled to room temperature and diluted with 0.5 L H_2O and left overnight. Then, the mixture was filtered and washed with H_2O using a 0.45 μm Millipore-filter to remove the residual acid. The product was dried under ambient condition. This pre-oxidized graphite was then subjected to oxidation by Hummers' method described as follows. Pretreated graphite powder was put into cold (0 °C) concentrated H_2SO_4 (120 ml). Then, $KMnO_4$ (15 g) was added gradually under stirring and the temperature of the mixture was kept to be below 20 °C by cooling. Successively, the mixture was stirred at 35 °C for 2 h, and then carefully diluted with 250 ml of H_2O. After that, the mixture was stirred for 2 h, and then additional 0.7 L of H_2O was added. Shortly, 20 ml of 30% H_2O_2 was added to the mixture. The resulting brilliant-yellow mixture was filtered and washed with 10 wt% HCl aqueous solution (1 L) to remove metal ions followed by washed repeatedly with H_2O to remove the acid until the pH of the filtrate was neutral. The GO slurry was dried in a vacuum oven at 60 °C and purified by dialysis for one week.

2.3. Preparation of GNS via reduction of GO

A fresh sample (200 mg) of GO solid was dispersed in 400 ml of H_2O with the aid of sonication using a high-power (800 W) ultrasonic pole at 0 °C for 60 min, followed by centrifugation at 3000 rpm for 15 min to remove a small quantity of precipitation, to form a black-brown GO aqueous colloid. This homogenous dispersion was tested to be stable for several months. In a typical reduction procedure from GO to graphene, 20 ml of GO colloid was mixed with 20 ml of H_2O, 17.5 μl of hydrazine solution (80 wt% in water), 313.6 μl of ammonia solution (25 wt% in water) in a 100 ml flask. After being vigorously stirred for 10 min, the mixture was refluxed at 95 °C for 2 h and cooled down to room temperature, forming a black graphene aqueous dispersion. The graphene dispersion was filtered and washed repeatedly with H_2O to remove the residual alkali compounds until the pH of the filtrate was neutral. The GNS powder was obtained by drying the filter solid in a vacuum oven at 60 °C over night.

2.4. Preparation of the CNF/GNS composite paper

In order to prepare electrospun precursor suspension, powdery GNS was dispersed in 50 g of DMF by pole-ultrasonication (600 W, 30 min) to form a uniform suspension. After that, 5.0 g of PAN was added into the suspension and kept stirring for 12 h to form the uniform precursor suspension. The weight ratio between PAN and GNS was 1:0.03.

This suspension was spun into a GNS/PAN fibrous paper using a home-made electrospinning equipment, which was consisted of a metal needle (the inert diameter of 0.5 mm) connected to the positive electrode of a DC high-voltage power supply, a syringe pump and a rolling graphite drum (the diameter of 4.0 cm) connected to the negative electrode of the same power supply. In a typical electrospinning process running at room temperature, the parameters for electrospinning were as follows: the applied electric voltage was 15 kV, the distance between the spinneret and the graphite drum was 15 cm, and the solution feed rate was 0.5 ml h^{-1}. The electrospun fibers were collected as a paper wrapped on the graphite drum with a rotation speed of 460 rpm min^{-1}. After 3 h of electrospinning, the graphite drum wrapped with PAN/GNS fibers was dried at room temperature over night. After that, the dried nanofibers were stabilized at 270 °C in air for 30 min and then peeled off from the drum to form a freestanding paper. This PAN/GNS composite paper was placed into a ceramic boat and transferred into a ceramic tube-furnace. At last, the CNF/GNS paper was prepared by heat-treatment at 900 °C for 2 h (the heating rate of 1 °C min^{-1}) under a high purity nitrogen atmosphere (99.99%).

In comparison, the same content of PAN was dissolved into another 50 g of DMF to form a precursor solution for electrospinning and subsequent heat-treatment under the same condition, to generate pure CNF paper.

2.5. Characterizations of the CNF paper and the CNF/GNS composite paper

The morphology and microstructure of the as-prepared GNSs were investigated by a FESEM (JSM-6701F) and a TEM (JEM-2010). The microstructure of the GNSs was investigated by a micro-Raman spectroscopy (JY-HR800, the excitation wavelength at 532 nm) and a Nanoscope III multimode atomic force microscope (AFM, Veeco) in tapping mode.

FESEM was also employed to investigate the morphology of the paper-like samples. X-ray diffraction (XRD) patterns were carried out by an X-ray diffraction using CuKα radiation (XRD, Philips X'Pert Pro.), to investigate the structure and compositions of the paper-like samples. Nitrogen adsorption isotherm measurements were

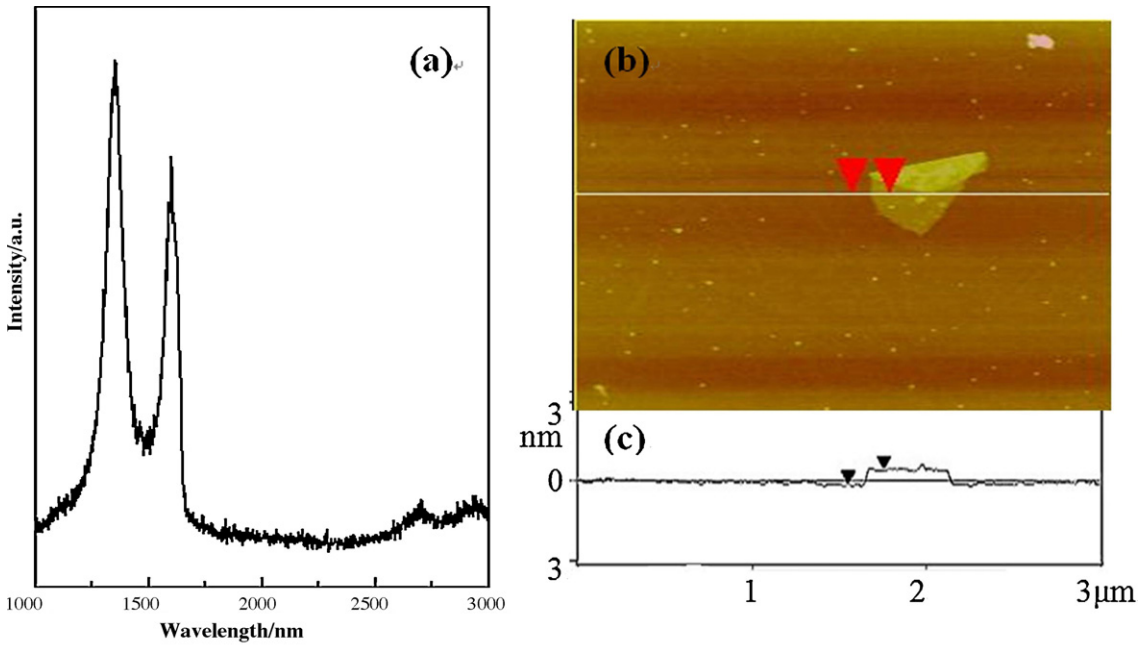

Fig. 1. Characterization of as-prepared GNSs: (a) Raman spectrum and (b) AFM image of an individual GNS and its height analysis.

performed on a Micromeritics ASAP 2020 volumetric adsorption analyzer at 77 K. The Brunauer–Emmett–Teller (BET) method was utilized to calculate the specific surface area of each sample.

2.6. Electrode preparation and electrochemical measurements

The electrochemical properties of the paper-like samples were carried out using Autolab Electrochemical Working Station (μAUTOLAB type III) in a conventional Teflon electrochemistry cell with a three-electrode system in 6 M KOH electrolyte at the room temperature: a working electrode (WE), a platinum wire counter electrode and a saturated calomel electrode (SCE). The CNF or the CNF/GNS composite paper was directly cut into 10 mm × 10 mm square and then pressed by a folded foamed nickel for a working electrode. Each carbon electrode contained about 1.1 mg of electroactive material. The cyclic voltammetry (CV) curves were collected with a potential window from −0.9 to −0.1 V (vs. SCE) at different scan rate ranging from 5 to 100 mV s^{-1}. Electrochemical impedance spectroscopy (EIS) measurements were recorded from 100 kHz to 100 MHz. Galvanostatic charge/discharge measurements were run on from −0.9 to −0.1 V at different current density, and open circuit potential. The capacitance was calculated from the slope of the discharge curve, according to the equation $C = (I \times \Delta t)/(\Delta V \times m)$, where C was the specific capacitance, I was the constant discharge current, Δt was the discharge time, ΔV was the voltage difference in discharge and m was the mass of the working electrode. The cycling stability test was evaluated with a Land CT2001A battery program-control test system (LAND, Wuhan, China).

3. Result and discussion

Raman spectroscopy is a fast and non-destructive method for the characterization of carbon materials. A typical Raman spectrum of GNS is showed in Fig. 1a. The spectrum exhibits two intense peaks at 1360 cm^{-1} and 1580 cm^{-1}, corresponding to the D and G bands, respectively. In addition, 2D band at 2700 cm^{-1} is also observed. The G band is related to the vibration of sp^2-hybridized carbon, whereas the D band corresponds to the sp^2-hybridized carbon with defects associated with vacancies, disorder and grain boundaries.

As Fig. 1b shows, the AFM image and its corresponding height profile show that an individual GNS on a silicon wafer surface has a thickness of 1 nm, which is accordant with the value for single-layer GNS sheet [27]. The measured thickness of the GNS is much larger than the theoretical value of graphene layer (0.34 nm), which is because that large quantity of oxygenous groups remains on the surface of GNS.

The obtained freestanding CNF/GNS paper has a black reflection under transmitted white light (Fig. 2a). Similar to the CNF paper, the CNF/GNS composite paper can be bent easily, suggesting good flexibility (seen inset of Fig. 2a). Fig. 2b shows the optical image of the 10 wt% DMF suspension of the PAN-GNS (the mass ratio of GNS to PAN is 0.03:1) after rest for one week. As shown in Fig. 2b, the suspension is homogeneous and stable for one week without any precipitation.

SEM analyses reveal that there is obvious difference in the morphology between the CNF paper and the CNF/GNS composite paper.

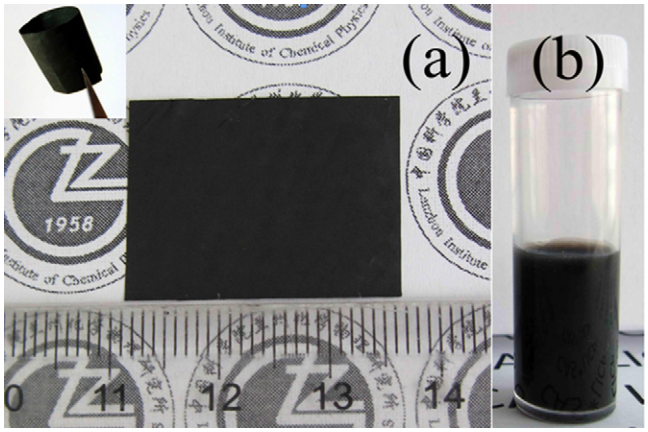

Fig. 2. (a) Digital camera image of the CNF/GNS composite paper. The inset image indicates its flexibility. (b) The optical image of the 10 wt% DMF suspension of the PAN-GNS (the mass ratio of GNS to PAN is 0.03:1) after rest for one week.

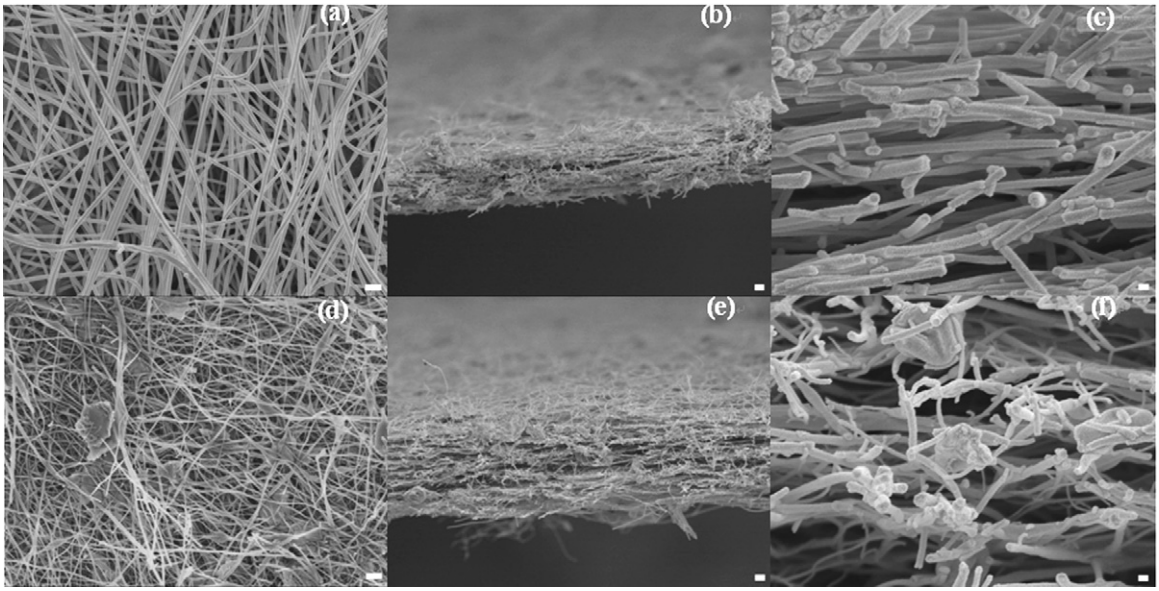

Fig. 3. Top-view SEM images of the CNF paper (a) and the CNF/GNS composite paper (d). Side-view SEM images of the CNF paper (b) and (c) and the CNF/GNS composite paper (e) and (f). The scale is 1 μm in (a), (b), (d) and (e), 100 nm in (c) and (f).

As shown in Fig. 3a–c, the CNF paper is composed of layer-by-layer overlapped and crossed nanofibers. In comparison, as shown in Fig. 3d–f, the CNF/GNS paper consists of layer-by-layer overlaps, and the GNSs are distributed uniformly among the CNFs forming a layer-by-layer 3D composite paper. In addition, the fracture edge of the CNF/GNS paper (Fig. 3f) also reveals that the GNSs are distributed throughout the entire cross-section of CNF layers. The cross-sections (Fig. 3b and d) of the two kinds of papers indicate that the thicknesses of the two types of paper are approximately 6 and 10 μm, respectively. Compared with the pure CNF paper, the diameter of the CNFs in CNF/GNS composite paper decreases, and the CNF/GNS paper is much fluffier and lighter than pure CNF paper.

Moreover, the XRD investigation results (Fig. 4) further confirm the successful introduction of GNS into the CNF paper. As shown in Fig. 4, the XRD pattern of the CNF paper exhibits one broad peak centered at $2\theta = 22.6^\circ$, indicating the amorphous nature. In comparison, there are two new peaks at $2\theta = 24.5^\circ$ and $2\theta = 42.8^\circ$ existing in the XRD pattern of the GNS/CNF composite paper, which are typical of GNS.

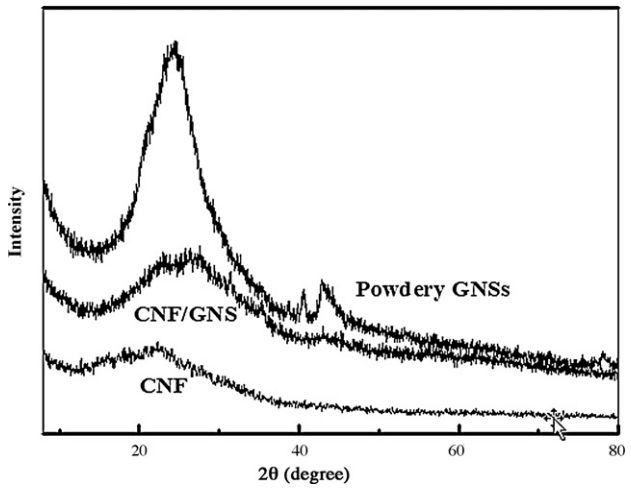

Fig. 4. XRD patterns of the CNF paper, the CNF/GNS composite paper and as-prepared powdery GNSs.

The surface area of ideal graphene was calculated to 2630 $m^2 g^{-1}$, hugely favorable for energy storage applications [14]. As a filler material, GNS was added to the CNF paper and may be in favor of increasing the surface area of the CNF/GNS composite. To prove this hypothesis, the specific surface area and pore-size analyses of the CNF, GNS, CNF/GNS samples were conducted using N_2 adsorption and desorption experiments. Table 1 summarizes the textural properties of the samples. Pure GNS exhibited an average pore size of 21.09 nm, and the BET surface area of GNS is 98 $m^2 g^{-1}$, which is accordance with the value of 106 $m^2 g^{-1}$ for hydrazine reduced GNSs reported by Chen et al. [28]. Pure CNF paper showed a specific surface area of 270.9 $m^2 g^{-1}$ and an average pore size of 10.68 nm. In comparison, after adding GNS, the specific surface area of the composites increased while the average pore sizes decreased. The CNF/GNS paper exhibited the highest specific surface area of 447 $m^2 g^{-1}$ and an average pore size of 8.16 nm. It also indicates that the CNF/GNS paper provides more contact area than CNF paper and GNSs with the electrolyte.

The electrical conductivity of the CNF, GNS and CNF/GNF paper is measured by a four pobe method, and the result is shown in Table 1. The conductivity of GNS paper was 2200 $S m^{-1}$, while the conductivity of CNF was 110 $S m^{-1}$, was several magnitudes lower than that of graphene. However, after adding GNS to CNF, the conductivity of CNF/GNS paper was 200 $S m^{-1}$, which much higher than that of pure CNF paper.

The electrochemical performances of the paper-like samples were analyzed using cyclic voltammetry (CV), galvanostatic charge/discharge, electrochemical impedance spectroscopy (EIS) and cycle-life test. Fig. 5a shows the CV curves GNS, CNF and CNF/GNS electrodes at a scan rate of 100 mV s^{-1} between −0.9 and

Table 1
Specific surface area, pore volume, pore size, specific capacitance and conductivity of the GNS, CNF and GNS/CNF.

Sample	S_{BET} ($m^2 g^{-1}$)	V_{total} ($cm^3 g^{-1}$)	P_w (nm)	Specific capacity ($F g^{-1}$)	Conductivity ($S m^{-1}$)
GNS	98	0.346	21.09	130	2200
CNF	277	0.184	10.68	159	111
GNS/CNF	463	0.253	8.16	197	200

S_{BET}: specific surface area; V_{total}: total pore volume; P_w: pore average pore diameter.

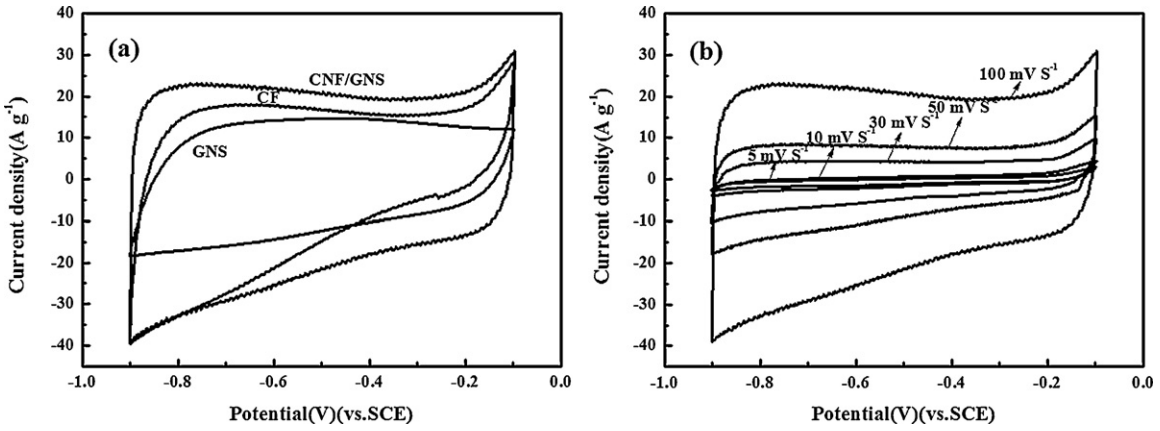

Fig. 5. CV curves of (a) pure GNS, CF and CNF/GNS electrode at sweep rate of 100 mV s^{-1} and (b) CNF/GNS electrodes at different scan rates.

−0.1 V (vs. SCE) in 6 M KOH aqueous electrolyte. It can be seen that the CV curves of all the electrodes show a typical rectangular shape and no obvious Faradaic current is observed in the voltammogram. Moreover, it is clear that the CNF/GNS electrode exhibits a larger CV area than that of the CNF and GNS electrode, indicating a higher specific capacitance compared with the pure CNF and GNS. This is probably due to that the well dispersed GNS in CNF provides a three-dimensional net work for electronic transmission, which would improve the connectivity of CNFs, the specific surface area, and the electrochemical utilization of pristine CNF during the charge/discharge process. Fig. 5b shows the CV curves of the CNF/GNS electrode at different scan rates. No obvious distortion in the CV curves is to be observed as the sweep rate increased, suggesting a highly reversible system in the KOH electrolyte within the potential range employed.

Fig. 6a shows the galvanostatic discharge curves of the GNS, CNF and CNF/GNS papers at the current density of 1.25 A g^{-1}. It is clearly seen that the shape of the discharge curves of the three electrode are closely linear and show a typical triangle symmetrical distribution, indicating a good double layer capacitive property. According to the capacitance equation, the specific capacitances of the GNS, CNF and CNF/GNS composite papers are 130, 159 and 197 F g^{-1}, respectively. These results suggested that the specific capacitance of the pristine CNF paper could be improved by introduction of GNSs.

As shown in Table 1, the pure CNF showed a specific surface area of 270.9 m^2 g^{-1} and an average pore size of 10.68 nm. In comparison, after adding GNS, the specific surface area of the composites increased while the average pore sizes decreased. The CNF/GNS paper exhibited the highest specific surface area of 447 m^2 g^{-1} and an average pore size of 8.16 nm. Moreover, the conductivity of CNF/GNS paper was 200 S m^{-1}, which was much higher than that of pure CNF paper. We believed that the high specific surface area, the suitable small pore size and the high conductivity of CNF/GNS electrode were in favor of the absorption and the transport of electrolyte ions through the porous channels within the CNF/CNF paper. Therefore, the highest specific capacitance of CNF/GNS electrode was mainly attributed to the high specific surface area and high conductivity.

To further understand the high rate capability of the CNF/GNS electrode, the chare/discharge measurements at different current densities were recorded. Fig. 6b displays the discharge curves of the CNF/GNS electrode on the current density in the range of 1.25–2 A g^{-1}. It can be clearly seen that the specific capacitance gradually decreases with the increase of the current density. Up to a relatively large current density of 2 A g^{-1}, nearly 86% of the initial value is remained for CNF/GNS electrode, indicating that the CNF/GNS paper electrode allows rapid ion diffusion [29].

EIS analysis is recognized as one of the principal methods examining the fundamental behavior of electrode materials for supercapacitors [1,30]. For further understanding, impedances of the GNS, CNF and CNF/GNS composite papers were measured in the frequency range of 10 kHz to 0.1 Hz at open circuit potential with an AC perturbation of 5 mV. As shown in Fig. 7, two impedance spectra are almost similar in form with an arc at a higher frequency region and a spike at a lower frequency region. The equivalent circuit in the inset of Fig. 7 is composed of five elements: the internal resistance (R_1), including the bulk electrolyte solution resistance, the intrinsic resistance of active material, and the electron transfer resistance at

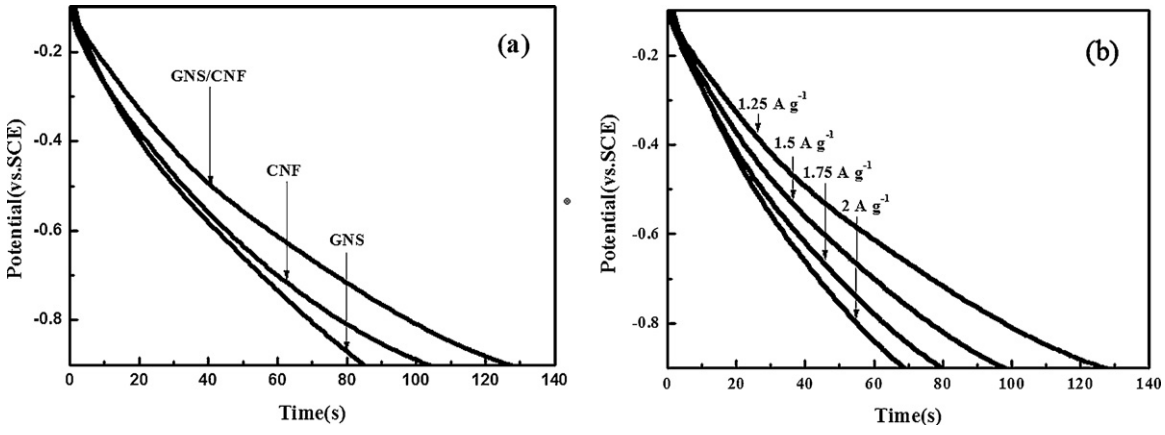

Fig. 6. Galvanostatic discharge curves of (a) pure GNS, CF and CNF/GNS electrode at 1.25 A g^{-1} and (b) CNF/GNS electrodes at different current densities.

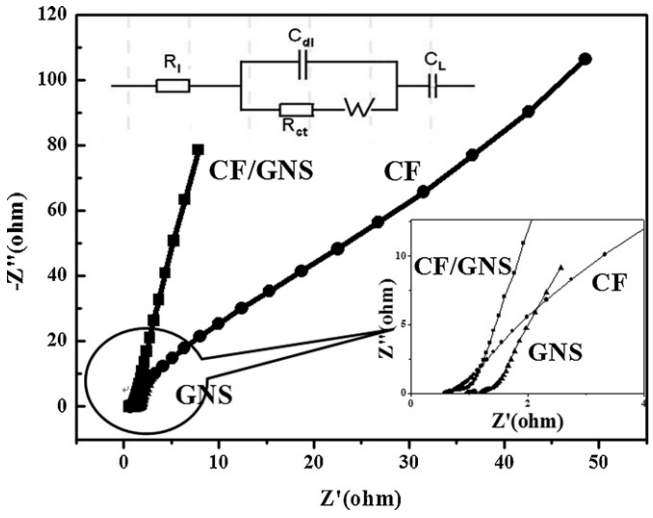

Fig. 7. Nyquist plots of experimental impedance data (scattering dot) and fitting results (solid line). The inset shows the electrical equivalent circuit used for fitting impedance spectra. The inset image is the equivalent circuit and the detail with enlarged scale.

current collector/electrode boundary [31]; the electrical double-layer capacitance (C_{dl}); the charge-transfer resistance (R_{ct}); the Warburg impedance (Z_W); and the pseudocapacitance (C_l). Clearly, the charge-transfer resistance and the Warburg impedance for the CNF electrode decreased because of adding GNS, the most possible reason is that the high temperature treatment make the containing oxygen functional groups on the GNSs surfaces reduces. Furthermore, GNS in the composite material is not only able to provide double-layer capacitance to the overall energy storage, but also efficient electron transfer channels to improve the electrochemical performance. What's more, it also can be found that for the GNSs the straight line of the impedance spectroscopy in the low frequency was obviously shorter than that of others materials. Song et al. have reported that the penetration depth of AC signal in the porous materials was strong dependence on the porous size [32]. The larger pore size of the materials and the more depth AC signal immersed into the materials result in the longer the straight part of impedance spectroscopy.

Long cycle life of supercapacitors is a crucial parameter for their practical applications [33]. The long-term cycle stability of the electrodes was likewise evaluated by repeating galvanostatic charge–discharge test between −0.9 and −0.1 V (vs. SCE) at a current density of 1.25 A g^{-1} for 1500 cycles (Fig. 8). It is clear seen that the specific capacitance of the CNF/GNS paper still remains above 165 F g^{-1} after 1500 cycles (about 84% of the original value), illustrating good stability and lifetime as the supercapacitor.

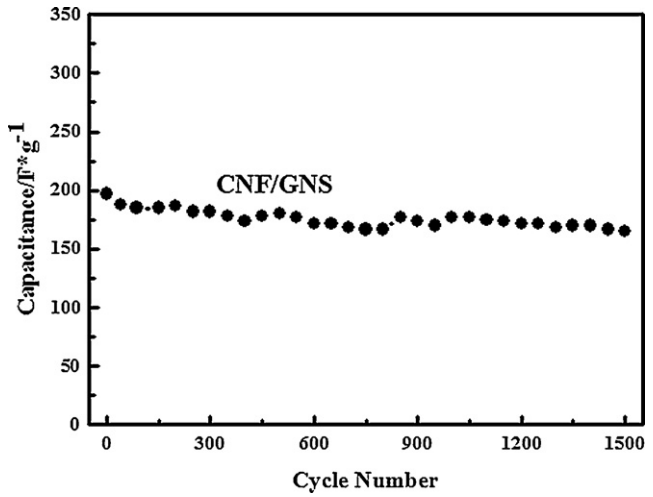

Fig. 8. Variation of the specific capacitances as a function of cycle number measured at 1.25 A g^{-1} for 1500 cycles.

4. Conclusions

In summary, a combination of electrospinning and thermal treatment has been successfully utilized to prepare freestanding CNF/GNS composite paper. The as-obtained composite paper maintains the pristine flexibility of the CNF paper, and displays remarkably improved BET surface area and electrochemical performances compared with the CNF paper and GNSs. The GNS/CNF composite paper exhibits the largest specific capacitance of 197 F g^{-1}, about 24% higher than that of pure CNF paper. Thus, the CNF/GNS composite paper is a potential low-cost candidate for use as flexible supercapacitors.

Acknowledgments

This work was supported by the Top Hundred Talents Program of Chinese Academy of Sciences, the National Basic Research 973 Program of China, the National Nature Science Foundations of China (51005225) and the Postdoctoral Science Foundation of China (20100480728).

References

[1] B.E. Conway, Modern Aspects of Electrochemistry, Plenum Press, New York, 1999.
[2] M.J. Pitkethly, Nano Today 7 (2004) 20.
[3] D.W. Wang, F. Li, J.P. Zhao, W.C. Ren, Z.G. Chen, J. Tan, Z.S. Wu, L. Gentle, G.Q. Lu, H.M. Cheng, ACS Nano 3 (2009) 1745–1752.
[4] F. Beguin, K. Szostak, G. Lota, E. Frackowiak, Adv. Mater. 17 (2005) 2380–2384.
[5] D.N. Futaba, K. Hata, T. Yamada, T. Hiraoka, Y. Hayamizu, Y. Kakudate, O. Tanaike, H. Hatori, M. Yumura, S. Iijima, Nat. Mater. 5 (2006) 987–994.
[6] M. Kaempgen, J. Ma, G. Gruner, G. Wee, S.G. Mhaisalkar, Appl. Phys. Lett. 90 (2007) 264104–264106.
[7] L.J. Ci, S.M. Manikoth, X.S. Li, R. Vajtai, P.M. Ajayan, Adv. Mater. 19 (2007) 3300–3303.
[8] C. Kim, Y.O. Choi, W.J. Lee, K.S. Yang, Electrochim. Acta 50 (2004) 883–887.
[9] L.W. Ji, Z.H. Lin, A.J. Medford, X.W. Zhang, Carbon 47 (2009) 3346–3350.
[10] E.J. Ra, E. Raymundo-Pinero, Y.H. Lee, F. Beguin, Carbon 47 (2009) 2984–2992.
[11] H.Q. Chen., M.B. Müller, K.J. Gilmore, G.G. Wallace, D. Li, Adv. Mater. 20 (2008) 3557–3561.
[12] Y. Zhu, S. Murali, W. Cai, X. Li, J.W. Suk, J.R. Potts, R.S. Ruoff, Adv. Mater. 22 (2010) 3906–3924.
[13] M.D. Stoller, S. Park, Y. Zhu, J. An, R.S. Ruoff, Nano Lett. 8 (2008) 3498–3502.
[14] C.G. Liu, Z.N. Yu, D. Neff, A. Zhamu, B.Z. Jang, Nano Lett. 10 (2010) 4863–4868.
[15] S.J. Biswas, L.T. Drzal, Chem. Mater. 22 (2010) 5667–5671.
[16] J. An, T. Wei, B. Shao, F. Ma, Z.J. Fan, M. Zhang, C. Zheng, Y.C. Shang, W.Z. Qian, F. Wei, Carbon 48 (2010) 1731–1737.
[17] X.B. Yan, J.T. Chen, J. Yang, Q.J. Xue, P. Miele, ACS Appl. Mater. Interfaces 2 (2010) 2521–2529.
[18] Y.X. Xu, H. Bai, G.W. Lu, C. Li, G.Q. Shi, J. Am. Chem. Soc. 130 (2008) 5856–5857.
[19] D. Li, M.B. Müller, S. Gilje, R.B. Kaner, G.G. Wallace, Nat. Nanotechnol. 3 (2008) 101–105.
[20] W. Yao, J. Yang, J. Wang, L. Tao, Electrochim. Acta 53 (24) (2008) 7326–7330.
[21] S.H. Kim, Y.I. Kim, J.H. Park, J.M. Ko, Int. J. Electrochem. Sci. 4 (2009) 1489–1496.
[22] X.B. Yan, Z.X. Tai, J.T. Chen, Q.J. Qun, Nanoscale 2 (2011) 212–216.
[23] M. Ates, A.S. Sarac, J. Appl. Electrochem. 39 (2009) 2043–2048.
[24] J.H. Kim, A.K.Y. Sharma, S. Lee, Mater. Lett. 60 (13–14) (2006) 1697–1701.
[25] Q.H. Guo, X.P. Zhou, X.Y. Li, S.L. Chen, A. Seema, A. Greiner, H. Hou, J. Mater. Chem. 19 (18) (2009) 2810–2816.
[26] C.T. Hsieh, W.Y. Chen, Y.S. Cheng, Electrochim. Acta 55 (19) (2010) 5294–5300.
[27] D. Li, M.B. Müller, G. Scott, R.B. Wallace, G.G. Kaner, Nat. Nanotechnol. 3 (2008) 101–105.
[28] D.W. Wang, F. Li, Z.S. Wu, W.C. Ren, H.M. Cheng, Electrochem. Commun. 11 (2009) 1729–1732.
[29] C. Kim, B.T.N. Ngoc, K.S. Yang, M. Kojima, Y.A. Kim, Y.J. Kim, M. Endo, S.C. Yang, Adv. Mater. 19 (2007) 2341–2346.
[30] W. Sugimoto, H. Iwata, K. Yokoshima, Y. Murakami, Y. Takasu, J. Phys. Chem. B 109 (2005) 7330–7334.
[31] Q.F. Wu, K.X. He, H.Y. Mi, X.G. Zhang, Mater. Chem. Phys. 101 (2007) 367–373.
[32] H.K. Song, Y.H. Jung, K.H. Lee, L.H. Dao, Electrochim. Acta 44 (1999) 3513–3519.
[33] J. Yan, T. Wei, W.M. Qiao, B. Shao, Q.K. Zhao, L.J. Zhang, Z.J. Fan, Electrochim. Acta 55 (2010) 6973–6978.